Resolving the true electrical conductivity using EM38 and EM31 and a laterally constrained inversion model

John Triantafilis[A], Fernando Monteiro Santos[B]

[A]School of Biological Earth and Environmental Sciences, University of New South Wales, Sydney, NSW, Australia, Email j.triantafilis@unsw.edu.au
[B]Universidade de Lisboa, Instituto Don Luís Laboratório Associado, C8, 1749-016 Lisboa, Portugal

Abstract
The ability to map the spatial distribution of average soil property values using geophysical methods at the field level has been well described. This includes the use of electromagnetic (EM) instruments which measure bulk soil electrical conductivity (σ_a). However, soil is a three-dimensional medium. In order to better represent the spatial distribution of soil properties with depth, methods of inverting σ_a data have been attempted (e.g. Tikhonov regularisation). In this paper we employ a 1-D inversion algorithm with 2-D smoothness constraints to predict true electrical conductivity (σ) using σ_a data collected along a transect in an irrigated field in the lower Namoi valley. The σ_a data includes the root-zone measuring EM38 and the vadose-zone sensing EM31: in the vertical (v) and horizontal (h) dipole modes and at heights of 0.2 and 1.0 m, respectively. In addition, we collected EM38 σ_a at heights of 0.4 and 0.6 m. In order to compare and contrast the value of the various σ_a data we carry out individual inversions of EM38v and EM38h collected at heights of 0.2, 0.4 and 0.6 m, and EM31v and EM31h at 1.0 m. In addition, we conduct joint inversions of various combinations. We find that the values of σ achieved along the transect represent the duplex nature of the soil. In general, the EM38 assists in resolving solum and root zone variability of the cation exchange capacity (CEC – cmol(+)/kg of soil solids) and the electrical conductivity of a saturated soil paste extract (EC_e – dS/m), whilst the use of the EM31 assists in characterising the vadose-zone and the likely location of a shallow perched-water table. In terms of identifying an optimal set of EM σ_a data for inversion we found that a joint inversion of the EM38 at a height of 0.6 m and EM31 signal data provided the best correlation with electrical conductivity of a saturated soil paste (EC_p – dS/m) and CEC (respectively, 0.81 and 0.77).

Key Words
Drainage channels, digital soil mapping, EM38, EM31, electromagnetic (EM) induction, EM inversion

Introduction
The application of electromagnetic (EM) induction instruments for digital soil mapping has increased over the last 10 years. For example, the EM38 has been used to map management zones (Triantafilis *et al.* 2009a) and map the spatial distribution of average soil moisture (Tromp van Meerveld and McDonnell 2009), soil salinity (Wu *et al.* 2009), deep drainage (Triantafilis *et al.* 2003), depth to water table (Buchanan and Triantafilis 2009), clay content (Triantafilis *et al.* 2001) and CEC (Triantafilis *et al.* 2009b).
However, management of soil requires information about the vertical distribution of its properties. In order to determine this, various approaches have been proposed. The best examples appear in relation to describing soil salinity. Australian examples include logistic profile modeling (Triantafilis *et al.* 2000). A less site-specific approach involves the reconstruction of the true electrical conductivity (σ) profile itself. Cook and Walker (1992) developed a method using linear combinations of σ_a measurements to estimate σ at a depth interval of interest. Borchers *et al*. (1997) and Hendrickx *et al*. (2002) used Tikhonov regularization for estimating σ within a soil profile. The aim of this study is to use EM imaging and σ_a collected by an EM38 and EM31 to infer the spatial distribution of soil properties related to σ_a across an irrigated cotton field in the lower Namoi valley. We compare these models qualitatively and quantitatively with estimated and measured soil laboratory data including: volumetric moisture content (θ); electrical conductivity of a saturated soil paste (EC_p – dS/m) and extract (EC_e - dS/m); clay content (%); and, cation exchange capacity (CEC - mmol(+)/kg of soil solids).

Methods
The study field is located 3 km southeast of Wee Waa (Figure 1) which is situated in the lower Namoi valley of northern New South Wales (30.24°S, 149.48°E). It is located at the northern edge of the Pilliga Scrub. A large drainage channel is evident at the northern end of the field.
EM data collection involved acquisition along a transect using a Mobile Electromagnetic Sensing System-

MESS (Triantafilis *et al.* 2002). Here EM38 measurements are made in the vertical (EM38v) and horizontal (EM38h) modes. Given the operating frequency (i.e. 14.5 kHz) and coil spacing (1.0 m), the depth of exploration is 1.5 and 0.75 m (McNeill 1990), respectively, when the instrument is placed on the ground. In this study we measure EM38v and EM38h σ_a at heights of 0.2, 0.4 and 0.6 m. The larger coil spacing (3.7 m) and smaller operating frequency (9.8 kHz) of the EM31 enable exploration depths of 6 and 3 m, when measured in the vertical (EM31v) and horizontal (EM31h) mode and 1.0 m (McNeill 1980), respectively.
The EM38 and EM31 σ_a is passed through a modified version of a 1-D laterally constrained method (i.e. EM34-2D) developed by Monteiro Santos (2004). We use a damping factor (λ) of 0.6 with inversions modelled onto a 2 m mesh spacing along the transect at depths of: 0.075, 0.15, 0.25, 0.35, 0.45, 0.55, 0.65, 0.75, 0.85, 0.95, 1.05, 1.17, 1.28, 1.40, 1.53, 1.67, 1.80, 1.95 and 2.1 m.
To validate the EM inversions, 9 sites are available along the transect: Site 22 in the south to site 14 in the north. These were chosen to account for the range of EM σ_a data values (Triantafilis *et al.* 2009b). At each site soil was sampled at 0.30 m depth increments to 2.1 m. The samples were analysed for: gravimetric soil moisture content (w - %), electrical conductivity of a saturated soil paste (EC_p - dS/m) and its extract (EC_e - dS/m) and the saturation percentage (SP). We calculate θ (cm^3/cm^3) from w x ρ, where we estimate bulk density (ρ- g/cm^3) using $\rho = 1.73 - 0.0067$ x SP (Rhoades *et al.* 1989). Particle size fraction is determined using the hydrometer method with the soil texture class and grade determined. We estimate cation exchange capacity (CEC - mmol(+)/kg) using a mechanical leaching device (Tucker 1974; Holmgren *et al.* 1977).

Results and Discussion

Figure 1 shows the spatial distribution of EM38 and EM31 σ_a measured in various modes of operation and at several heights along transect 3. The following points summarize the σ_a data: i) σ_a patterns are similar; ii) σ_a is larger in the vertical than the horizontal mode for both instruments; iii) EM31 σ_a is larger than equivalent EM38 σ_a; iv) EM38 data decreases with increasing height: v) σ_a generally decreases from south to north (i.e. tail ditch); vi) Difference in σ_a in vertical and horizontal mode is larger in the south.
Figure 2a shows the plot of estimated volumetric soil water content (θ) with depth. Topsoil and subsurface clay is small (< 20 %) and equates to a loam to silty loam texture class (Texture Group - 3). At the southern end subsoil clay content (i.e. 22, 21, 20 and 19) is intermediate (i.e. 25-40 %) varying from a clay loam (Texture Group - 4) to light clay (Texture Group - 5). In the centre and north (i.e. 18, 17, 16, 15 and 14) subsoil clay (> 40 %) falls within the light-medium to heavy clay class (Texture Group - 6).

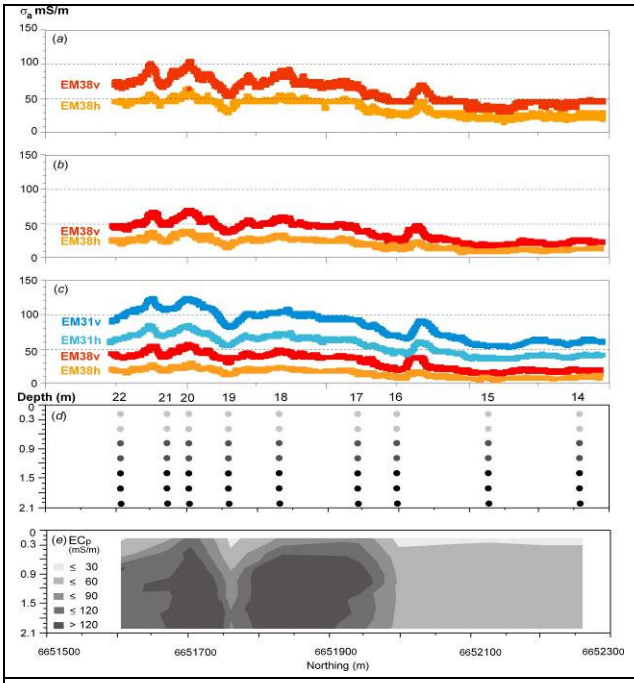

Figure 1. Spatial distribution of apparent soil electrical conductivity (σ_a - mS/m) of EM38v and EM38h and heights of: (a) 0.2 m, (b) 0.4 m; and, (c) 0.6 m and EM31v and EM31h at a height of 1.0 m; (d) location of 9 soil sampling sites along the transect; and, (e) electrical conductivity of saturated soil paste (EC_p - dS/m).

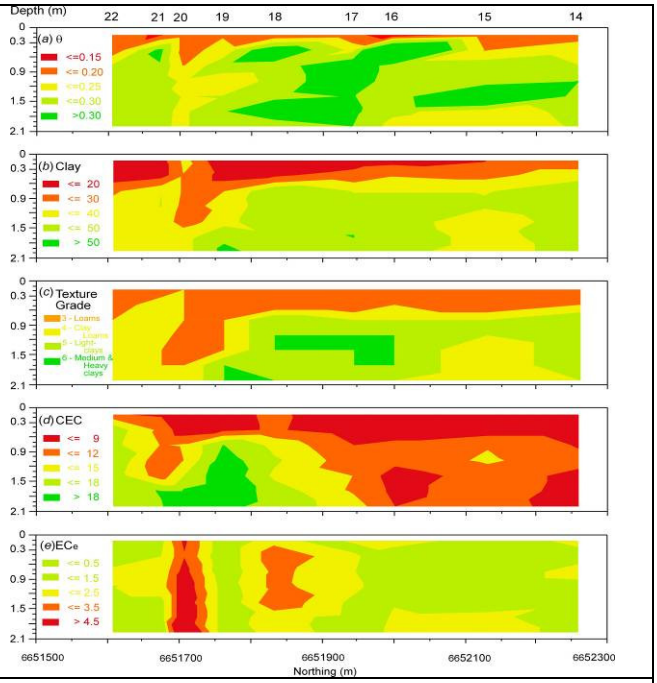

Figure 2. Contour plot of measured a) estimated volumetric moisture content (θ - cm^3/cm^3), b) clay content (%), c) soil texture grade, d) cation exchange capacity (CEC - cmol(+)/kg of soil solids), and e) electrical conductivity of saturated soil paste extract (EC_e - dS/m).

Figure 2d shows the topsoil is characterized by uniformly small CEC (i.e. < 9 cmol(+)/kg of soil) with CEC intermediate to large in the subsoil. At the southern end subsoil CEC is largest (i.e. > 18 cmol(+)/kg of soil), whilst in the north CEC ranges from small (9 cmol(+)/kg of soil) to intermediate (12-15 cmol(+)/kg of soil). With regard to EC_e, Figure 2e shows a small amount of salt has accumulated in two of the cores at the southern end. Interestingly site 19 exhibits salt levels equivalent to the profiles at the northern end (i.e. < 1.5 dS/m). Figure 1e shows measured EC_p. It represents the overall σ of the samples collected and is therefore a measure of the various soil properties known to influence σ_a. Figure 3a, b and c shows the spatial distribution of σ considering the inversion of the EM38 σ_a data at a height of 0.20, 0.4 and 0.6 m, respectively. The 2-D distribution of σ reflects the spatial distribution of θ and the duplex nature of the soil. The pattern of σ corresponds better with spatial distribution of CEC, EC_e and EC_p. The sandy to loamy sand topsoil (0-0.3 m) and subsurface (0.3-0.6 m) horizons are characterized by smaller σ (< 30 mS/m). At the northern end, intermediate-large σ (60-120 mS/m) characterize the medium clay textured subsoil horizon. Interestingly, the largest σ values (>120 mS/m) characterize equivalent medium clay and clay loam textured subsoil horizons in the centre and southern end, respectively. This is because the subsoil is more reactive, as evidenced by larger values of CEC (Figure 2d).

It is also worth mentioning that given the soil profiles along most of the transect are duplex in nature, we might have expected to resolve a sharp change in σ at a depth of around 0.30 m. The change in σ is gradual, however, with topsoil and subsurface σ (30 mS/m) changing to larger values in the subsoil (> 120 mS/m) over a depth range of 0.6 m. Nevertheless, the inversion of the EM38 σ_a data has been able to detect the extent of a known minor drainage channel at 6651750 and represented by the slot of small to intermediate values of profile σ (90-120 mS/m). This location is aligned with soil sampling site 19. In addition, a second minor drainage channel may also have been identified at 6651650.

To represent the spatial distribution of σ within the solum, we conducted various joint inversions. Figure 3d shows the σ profile achieved using the EM38 σ_a at heights of 0.4 and 0.6 m. The change in σ occurs over a smaller depth. An explanation is that as the EM38 is raised a larger proportion of the measurement is contributed by the less reactive topsoil and subsurface. However, the deep subsoil representation of soil is diminished, as is our ability to differentiate the clay mineralogy at either end of the field.

The deeper subsoil is better represented when we invert the EM31 data (Figure 3e). The large values of σ that characterise the deeper subsoil at the southern end of the field may be attributable to the presence of a shallow perched water table. Our ability to resolve topsoil and subsurface features are poor, however.

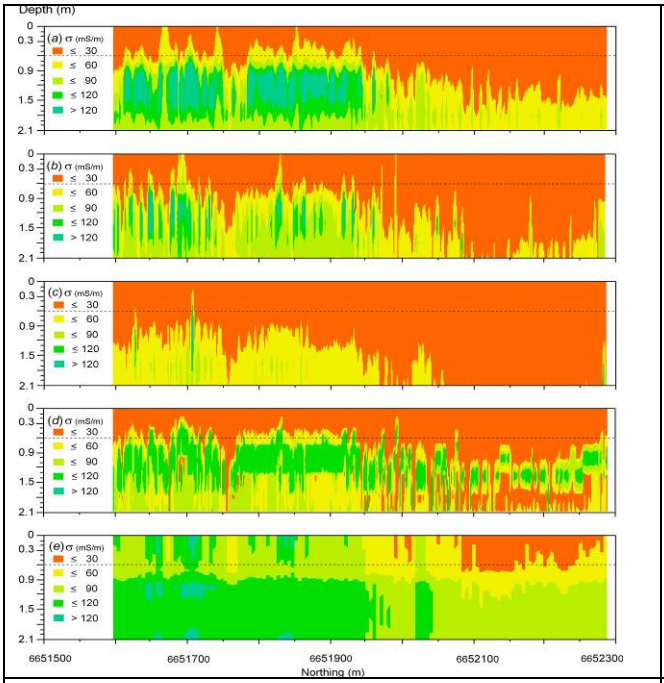

Figure 3. True electrical conductivity (σ - mS/m) estimated using apparent soil electrical conductivity (σ_a - mS/m) data collected using: an EM38 at a height of (a) 0.2 m, (b) 0.4 and (c) 0.6 m; and (d) joint inversion using the EM38 at heights of (d) 0.4 and 0.6 m, and (e) collected using only an EM31 at a height of 1.0 m.

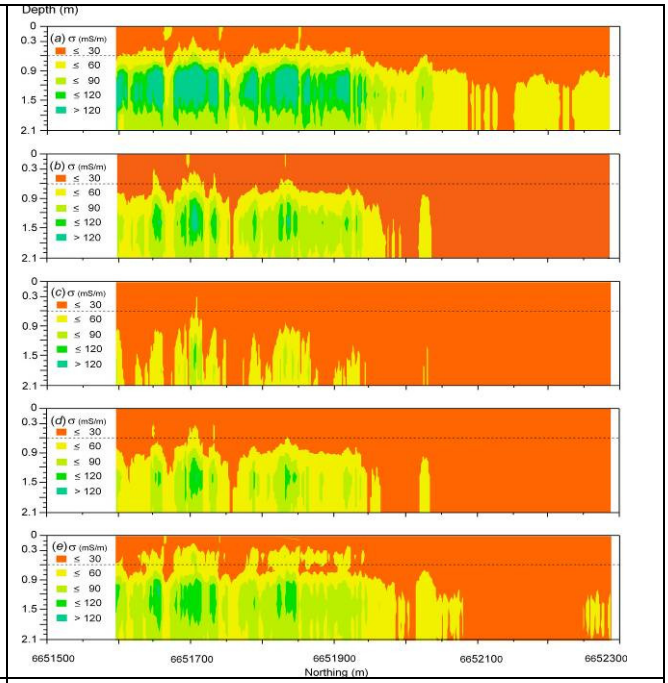

Figure 4. True electrical conductivity (σ - mS/m) estimated using apparent soil electrical conductivity (σ_a - mS/m) data collected using an EM31 at a height of 1.0 m and an EM38 at a height of (a) 0.2 m, (b) 0.4 and (c) 0.6 m; and joint inversions with the EM38 at heights of (d) 0.4 and 0.6 m, and (e) 0.2 m, 0.4 and 0.6 m.

The spatial distribution of σ developed from joint inversions between the EM31 and EM38 at individual heights of 0.2, 0.4 and 0.6 m are shown in Figure 4a, 4b and 4c, respectively. Joint inversions are also shown for various other combinations. In terms of determining an optimal set of σ_a data, we found that the use of the EM38 σ_a at a height of 0.6 m and EM31 data (Figure 4c) led to the highest correlation with EC_p (0.81).

Conclusion

The spatial distribution of topsoil, subsurface and subsoil properties are discernible by the inversion of σ_a data collected along an intensively surveyed transect within an irrigated cotton growing field south-east of Wee Waa. The root-zone model, where the EM38 σ_a data (EM38v and EM38h) available at heights of 0.20, 0.4 and 0.6 m discern the major soil types and physiographic features within the field. This includes: the duplex soil profiles with more reactive clay (> 12 cmol(+)/kg) at the southern end of the field and the duplex soil profiles associated with a prior stream at the northern end. The location of two minor drainage channels, equivalent to the soil that characterises the northern end are discerned at the southern end.

To better resolve the duplex nature of the soil we develop a solum model, which involved passing the entire EM38 σ_a data set (EM38v and EM38h) available at various heights (0.20, 0.40 and 0.60 m) through our 1-D inversion algorithm. Whilst we are able to better represent the clear and abrupt change in clay content, the inversion model is unable to resolve differences in subsoil σ of the two types of soil profile that characterize the northern and southern end of the field. The use of the EM31 σ_a data in reconstructing σ in the root-zone appears to be limited. Its greatest contribution is in characterizing and defining the lower boundary. This conclusion is borne out when we developed two joint EM inversion models of the soil and vadose-zone (e.g. developed by entering the EM38v and EM38h σ_a data available at various heights. Statistical analysis showed that the best correlation with EC_p (0.81) is achievable by jointly inverting the EM38 σ_a at a height of 0.60 m with the EM31 σ_a data. The approach we have used has been applied to the joint inversion of EM38 and EM34 σ_a data (Triantafilis and Santos 2009) as well as to a DUALEM-421 (Monteiro Santos *et al.* 2009).

References

Borchers B, Uram T, Hendrickx JMH (1997). Tikhonov regularization of electrical conductivity depth profiles in field soils. *Soil Science Society of America Journal* **61,** 1004-1009.

Buchanan SM, Triantafilis, J (2009) Mapping water table depth using geophysical and environmental variables. *Ground Water* **47,** 80-96.

Cook PG, Walker GR (1992) Depth profiles of electrical conductivity from linear combinations of electromagnetic induction measurements. *Soil Science Society of America Journal* **56,** 1015-1022.

Hendrickx JMH, Borchers B, Corwin DL, Lesch SM, Hilgendorf AC, Schlue J (2002). Inversion of soil conductivity profiles from electromagnetic induction measurements: Theory and experimental verification. *Soil Science Society of America Journal* **66,** 673-685.

Holmgren GGS, Juve RL, Geschwender RC (1977) A mechanically controlled variable leaching device. *Soil Science Society of America Journal* **41,** 1207-1208.

McNeill JD (1980) Electromagnetic terrain conductivity measurements at low induction numbers. Technical note TN-6, Geonics Limited, Mississauga Ontario, Canada.

McNeill JD (1990) Geonics EM38 Ground Conductivity Meter: EM38 Operating Manual. Geonics Limited, Mississauga Ontario, Canada.

Monteiro Santos FA (2004) 1-D laterally constrained inversion of EM34 profiling data. *Journal of Applied Geophysics* **56,** 123-134.

Rhoades JD, Manteghi NA, Shouse PJ, and Alves WJ 1989 Soil electrical conductivity and soil salinity: New formulations and calibrations. *Soil Science Society of America Journal* **53**, 433–439.

Monteiro Santos FA, Triantafilis J, Bruzgulis, KE, Roe JAE (2010). Inversion of DUALEM-421 profiling data using a 1-D laterally constrained algorithm. *Vadose Zone Journal* **9,** 117-125.

Tucker BM (1974) Laboratory procedure for cation exchange measurements in soils. CSIRO Division of Soils, Technical Paper No 23. (CSIRO, Australia).

Triantafilis J, Monteiro Santos FA (2009). 2-dimensional soil and vadose zone representation using an EM38 and EM34 and a laterally constrained inversion model. *Australian Journal of Soil Research* **47,** 809-920.

Triantafilis J, Laslett GM, McBratney AB (2000) Calibrating an electromagnetic induction instrument to measure salinity in soil under irrigated cotton. *Soil Science Society of America Journal* **64,** 1009-1017.

Triantafilis J, Huckel AI, Odeh IOA (2001) Comparison of statistical prediction methods for estimating field-scale clay content using different combinations of ancillary variables. *Soil Science* **166,** 415-427.

Triantafilis J, Ahmed MF, Odeh IOA (2002) Application of a mobile electromagnetic sensing system (MESS) to assess cause and management of soil salinisation in an irrigated cotton-growing field. *Soil Use Management* **18,** 330-339.

Triantafilis J, Huckel AI, Odeh IOA (2003) Field-scale assessment of deep drainage risk. *Irrigation Science* **21,** 183-192.

Triantafilis J, Kerridge B, Buchanan SM (2009a) Digital soil-class mapping from proximal and remotely sensed data at the field level. *Agronomy Journal* **101,** 841-853.

Triantafilis J, Lau KL, Buchanan SM (2009b). Field level digital soil mapping of cation exchange capacity using electromagnetic induction and a hierarchical spatial regression model in the lower Namoi Valley, Australia. *Australian Journal of Soil Research* **47,** 651-663.

Tromp-van Meerveld J, McDonnell JJ (2009) Assessment of multi-frequency electromagnetic induction for determining soil moisture patterns at the hillslope scale. Journal of Hydrology **368,** 56-67.

Tucker BM (1974) Laboratory procedure for cation exchange measurements in soils. CSIRO Australia, Division of Soils. Technical Paper No. 23. CSIRO, Australia.

Wu YK, Yang JS, Li XM (2009) Study on spatial variability of soil salinity based on spectral indices and EM38 readings. *Spectroscopy and Spectral Analysis* **29,** 1023-1027.